Journal of Sound and Vibration (1999) **221**(4), 681–708
Article No. jsvi1999.2030, available online at http://www.idealibrary.com on IDEAL

HIGH FREQUENCY RAY ACOUSTICS MODELS FOR DUCT SILENCERS*

A. CUMMINGS
School of Engineering, University of Hull, Hull HU6 7RX, U.K.

(*Received* 26 *May* 1998, *and in final form* 26 *October* 1998)

Hybrid modal/ray acoustics models for high frequency multimode sound propagation through finite-length dissipative duct silencers are being investigated and in this paper, the very simplest of these—involving no mean fluid flow, two-dimensional sound propagation, a locally reacting duct liner and no area change in the silencer—is described. A mode-matching scheme is also presented. Numerical predictions of silencer attenuation from the hybrid model and the mode-matching model are compared to experimental data taken from a two-dimensional silencer apparatus, and favourable agreement is noted. Above a certain lower frequency limit, the hybrid mode/ray model gives a good approximation for the silencer attenuation, in comparison to mode-matching predictions. Wave diffraction effects at the silencer terminations are also discussed.

1. INTRODUCTION

In predictive models for the acoustic attenuation of dissipative duct silencers both with and without mean fluid flow, it has often been assumed (see e.g., the paper by Cummings and Sormaz [1]) that the axial attenuation rate of the least attenuated acoustic mode will give a reasonable—possibly conservative—estimate of the silencer performance. Other, more complete, models (e.g., those of Mechel [2, 3], Sormaz *et al.* [4], for finite length silencers without flow and Sormaz [5] for such silencers with flow) involve mode-matching at the silencer's terminations, and allow for a specified multimode incident sound field. Finite element analysis and other numerical methods such as the method of weighted residuals have also been applied to finite length silencers, for example by Astley and Eversman [6] (in which a finite element formulation of the problem in the absence of mean gas flow is discussed), Eversman and Astley [7] (concerning a weighted residual method for the problem with mean flow) and Astley and

*Some of the material in this paper is included in a paper in the *Proceedings of the* 5*th International Congress on Noise and Vibration*, Adelaide, Australia, 15–18 December 1997.

0022–460X/99/040681 + 28 $30.00/0

Eversman [8] (involving a finite element scheme for the problem with mean flow). More recently, Kirby [9] has applied a three-dimensional finite element method to automotive silencers. Either mode-matching or fully numerical schemes can require considerable computational effort, and there may be some difficulty in identifying and tracking modes in the former case. At high frequencies, where there are many incident modes, the problem may become intractable and one is led to wonder whether a simpler approach, such as ray acoustics, can produce results of acceptable accuracy.

Ray models for duct acoustics have been investigated by several workers, such as Tester [10, 11], Kempton [12, 13] and Boyd *et al.* [14]. Tester [10] compared ray acoustics and modal predictions of the sound field from a two-dimensional line source in a duct with zero flow and locally reacting walls, and concluded that the ray acoustics models were "surprisingly" accurate. Kempton [13] compared mode theory and ray theory predictions of the insertion loss of a fan jet engine inlet silencer to measured data and noted good agreement under certain conditions, though he concluded that further research on interference and diffraction effects in the ray theory was needed. Boyd *et al.* [14] later presented ray theory predictions in which these effects were taken into account for a two-dimensional duct with zero flow, and noted generally good agreement with other results.

The attractive features of ray models are their simplicity and versatility, in application to difficult duct geometries. Computational "robustness" and rapidity are also features which can characterise such models. In the case of rectangular section duct silencers where uniform inlet and outlet ducts ensure well-defined modal sound fields, there are additional advantages in ray formulations, because a specified sum of propagating incident modes can readily be expressed as a sum of travelling wave components (or rays), and a transmitted ray field can—in suitable cases—equally easily be expressed as modes. Furthermore, it is often straightforward to find the incident modal field from a known source distribution. This case is—as it were—tailor-made for a ray treatment, in contrast to the general case where rather more elaborate ray-tracing methods may need to be applied (Dougherty [15], for example, described recent work on a ray-tracing technique designed for use in jet engine inlet ducts). It is, incidentally, worth noting that Mechel [2] resolved the incident and transmitted mode fields of a baffle type silencer into plane travelling wave components as a crucial part of his analysis, though these sound fields were matched to a modal sound field within the silencer itself.

In this paper, a very simple mode/ray formulation for sound attenuation in a finite length dissipative silencer with locally reacting walls, no area change and containing zero flow is described, and the results are compared to those from a mode-matching treatment and to measured data. Some attention is also paid to wave diffraction effects at the silencer terminations and to their role in determining the validity of the ray model. The results of these comparisons indicate the likely usefulness of ray models in more complex situations, such as silencers with area changes and mean fluid flow.

2. A HYBRID MODE/RAY MODEL FOR A DISSIPATIVE SILENCER

In the simple ray model described here, scattering effects at the silencer terminations are ignored, although their limiting effects on the validity of the model are discussed separately. Inclusion of these effects would negate the inherent simplicity of the ray model and incur great additional complexity. An essential and important difference between the present model and those described in references [10–15] is that, while in these other ray formulations rays are "traced" from a source to an observation point *via* reflections from the duct walls, the present treatment involves the generation of an incident modal sound field by a prescribed source distribution. These modes are then individually decomposed into rays until they have passed through the silencer, and the emerging rays are then recombined to construct a transmitted modal sound field.

2.1. THE MODEL

In Figure 1 is shown a section of two-dimensional duct with a length L of soft, locally reacting, walls (the "silencer", region 2) and rigid inlet and outlet sections (regions 1 and 3, respectively). The duct is—for convenience—assumed to be anechoically terminated at both ends. A simple-harmonic multimode sound field of radian frequency ω is incident from the left, and is assumed to consist of a sum of propagating modes comprising the plane wave (or fundamental) mode and a series of higher-order modes. The higher-order incident modes will be discussed first. Each of these modes may be represented as a combination of two plane travelling waves (treated here as rays) inclined to the duct axis, and one ray path—for a single mode—is shown. The other ray path for this mode consists of a vertical mirror image of that depicted, and this may readily be shown as follows. Suppose the incident sound field is given as a sum of modes by

$$p(x, y;\ t) = \mathrm{e}^{\mathrm{i}\omega t} \sum_{m=0}^{\infty} P_m \mathrm{e}^{-\mathrm{i}k_m x} \cos(m\pi y/a), \tag{1}$$

where $m(= 0,\ 1,\ 2, \ldots)$ is the mode order and k_m the axial wavenumber, $\sqrt{[k^2-(m\pi/a)^2]}$, k being the acoustic wavenumber, ω/c, and c the sound speed. Each mode may be represented as the sum of two travelling waves (or rays):

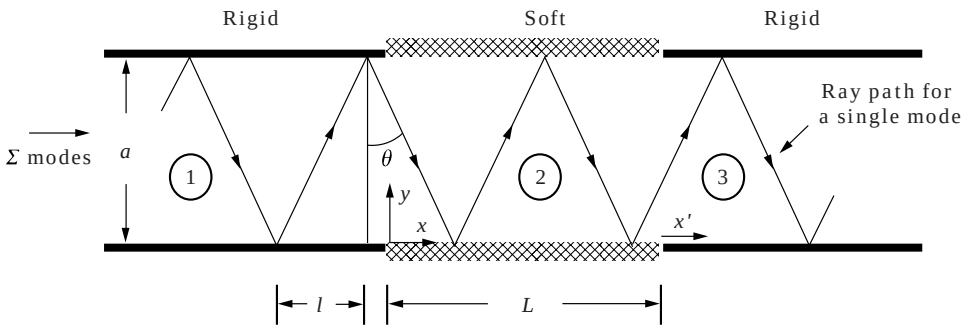

Figure 1. Finite length duct silencer with ray path.

$$P_m \cos(m\pi y/a) \exp(-\mathrm{i}k_m x) = (P_m/2)(\mathrm{e}^{-\mathrm{i}kx\sin\theta - \mathrm{i}ky\cos\theta} + \mathrm{e}^{-\mathrm{i}kx\sin\theta + \mathrm{i}ky\cos\theta}) \quad (2)$$

The component rays of each mode propagate at angle $\theta = \cos^{-1}(m\pi/ka)$ to the y-axis. This representation is equally valid in the transmitted sound field, but not in the silencer section, where the mode functions involve complex transverse wavenumbers. Suppose one neglects any diffraction effects at the silencer inlet and outlet (see sections 2.2 and 5.3 for a discussion of these effects), and assumes that purely specular reflection (at angle θ) of the rays occurs within both the rigid and soft duct sections. A ray leaving the rigid-walled inlet section strikes the soft walls in region 2 also at angle θ, and thereafter remains inclined at the same angle. This assumption will (as will be shown) become progressively better as the frequency increases. It is worth noting at this point that, while a single mode in regions 1 and 3 may be represented exactly by two component rays undergoing multiple reflections from the walls, the same does not hold for region 2. Morse and Ingård [16] (see Chapter 9) have shown that, for an appropriately large wall impedance, the two-ray modal synthesis is only approximately valid for lined ducts and comment, "An approximate answer is all we can expect from this mixture of wave and geometrical acoustics". One would therefore expect a single incident mode (or its two component rays) at angle θ from region 1 to excite a *series* of modes in region 2 (and *not* just a single mode) which—at sufficiently high frequencies—should combine to give an *approximation* to a multiply reflecting pair of rays at angle θ, with an equivalent net axial decay rate and phase speed, over the length of the lined duct section. The quality of this approximation would depend on the extent to which the assumptions of ray acoustics as applied here (e.g., negligible scattering effects) were satisfied.

If the *dimensionless* normal impedance of the soft walls (referred to the characteristic impedance of air and equal for both walls) is $z_w = r_w + \mathrm{i}x_w$, one may easily show that the sound power reflection coefficient of a ray from the duct walls is

$$\tau_\theta = [(r_w \cos\theta - 1)^2 + (x_w \cos\theta)^2]/[(r_w \cos\theta + 1)^2 + (x_w \cos\theta)^2]. \quad (3)$$

For a particular mode, the average number of reflections of its plane-wave components from the duct walls within the length L is $n = L/a \tan\theta$. Then the space-averaged mean-squared sound pressure of the mode at the silencer outlet is given in terms of that at the inlet by

$$\langle\overline{p_m^2}\rangle_{out} = \tau_\theta^n \langle\overline{p_m^2}\rangle_{in}, \quad m > 0, \quad (4)$$

since $\langle\overline{p_m^2}\rangle$ in a mode is the sum of $\langle\overline{p_m^2}\rangle$ in both component rays. The fundamental mode (with $m = 0$) must be treated separately because—according

to the above reasoning—its ray equivalent suffers no reflections from the duct walls and is therefore not attenuated as it passes through the silencer. This would lead to an under-prediction of the silencer attenuation, particularly in the case of long silencers, since all higher modes would experience attenuation in proportion to the length of the silencer, but the fundamental mode would not. Of course, the usual full "wave" treatment (involving a solution of the acoustic wave equation subject to the boundary conditions at the wall, see section 3) for the fundamental mode is incompatible with a ray model, but a simple quasi-plane wave treatment would seem appropriate in the present context, and will therefore be employed. Morse and Ingård [16] (Chapter 9) have described approximations to modal axial wavenumbers in ducts with small admittance walls and, for the fundamental mode, their results may be expressed as a fundamental mode propagation coefficient

$$\Gamma_0 = \Gamma_0^r + \mathrm{i}\Gamma_0^i = \mathrm{i}k\sqrt{1 - \mathrm{i}2/kaz_w}, \tag{5}$$

where the x-dependence in the fundamental mode is $\exp(-\Gamma_0 x)$. The real part of Γ_0 determines the axial attenuation rate of this mode, and one has

$$(\overline{p_0^2})_{out} = \exp(-2\Gamma_0^r L)(\overline{p_0^2})_{in} \tag{6}$$

as the equivalent of equation (4). Equation (5) will only yield a reasonably accurate prediction of the fundamental mode attenuation at fairly low frequencies, but it would normally be sufficient to suppress the dominating effect of this mode in cases where the higher modes present are fairly strongly attenuated.

It is of interest to be able to predict both the multimode sound pressure level difference LPD between the y-space-averaged mean-squared pressures at the silencer inlet and outlet (equal—in this model where there are no reflected waves—to IL, the insertion loss) and the sound power transmission loss TL, defined in the usual way. Both quantities will, of course, depend on the relative amplitudes of the modes in the incident sound field. Various assumptions may be made about this modal distribution, and some of them shall be considered in the following sub-sections.

2.1.1. *Equal mean-squared sound pressure and energy density in the incident modes*

Perhaps the simplest assumption is that $\langle\overline{p_m^2}\rangle_{in}$ is independent of m. (It is readily shown that this also implies that the modal energy density—defined as modal sound power per unit cross-sectional area of duct, divided by modal group velocity—is constant over all modes.) The y-space-averaged mean-squared pressure in the multimode inlet sound field is given simply as the sum of the space-averaged modal mean-squared pressures, over the number of propagating modes $N = \mathrm{Int}(ka/\pi) + 1$ ($\mathrm{Int}(x)$ signifying truncation to the value of the largest integer less than or equal to x), since cross-terms between modes integrate to

zero in the spatial averaging. From this assumption about the incident sound field, one has the result

$$\begin{aligned} LPD &= 10\log\left(\sum_{m=0}^{N}\langle\overline{p_m^2}\rangle_{in}\Big/\sum_{m=0}^{N}\langle\overline{p_m^2}\rangle_{out}\right)\\ &= 10\log\left(\sum_{m=0}^{N}\langle\overline{p_m^2}\rangle_{in}\Big/\left[\langle\overline{p_0^2}\rangle_{in}\exp(-2\Gamma_0^r L)+\sum_{m=1}^{N}\tau_\theta^n\langle\overline{p_m^2}\rangle_{in}\right]\right)\\ &= -10\log\left\{\frac{1}{N+1}\left[\exp(-2\Gamma_0^r L)+\sum_{m=1}^{N}\left(\frac{[(r_w-ka/m\pi)^2+x_w^2]}{[(r_w+ka/m\pi)^2+x_w^2]}\right)^{\frac{L}{a\sqrt{(ka/m\pi)^2-1}}}\right]\right\}. \end{aligned} \tag{7}$$

The TL may be found by summing the incident and transmitted modal sound power W_m per unit width of duct,

$$\begin{aligned} TL &= 10\log\left(\sum_{m=0}^{N}W_m^{in}\Big/\sum_{m=0}^{N}W_m^{out}\right)\\ &= 10\log\left(\sum_{m=0}^{N}W_m^{in}\Big/\left[W_o^{in}\exp(-2\Gamma_0^r L)+\tau_\theta^n\sum_{m=1}^{N}W_m^{in}\right]\right)\\ &= -10\log\left\{\frac{\exp(-2\Gamma_0^r L)+\sum_{m=1}^{N}\left[1-\left(\frac{m\pi}{ka}\right)^2\right]^{1/2}\left[\frac{(r_w-ka/m\pi)^2+x_w^2}{(r_w+ka/m\pi)^2+x_w^2}\right]^{\frac{L}{a\sqrt{(ka/m\pi)^2-1}}}}{\sum_{m=0}^{N}\left[1-\left(\frac{m\pi}{ka}\right)^2\right]^{1/2}}\right\}, \end{aligned} \tag{8}$$

since

$$W_m^{in}=\langle\overline{p_m^2}\rangle_{in}\frac{a}{\rho c}\frac{k_m}{k}\quad\text{and}\quad W_m^{out}=\tau_\theta^n W_m^{in}. \tag{9}$$

2.1.2. *Equal sound power in the incident modes*

The assumption here is that W_m^{in} is independent of m. Proceeding as above and utilising equation (9), one has

$$LPD=-10\log\left\{\frac{\exp(-2\Gamma_0^r L)+\sum_{m=1}^{N}\left[\frac{(r_w-ka/m\pi)^2+x_w^2}{(r_w+ka/m\pi)^2+x_w^2}\right]^{\frac{L}{a\sqrt{(ka/m\pi)^2-1}}}\left[1-\left(\frac{m\pi}{ka}\right)^2\right]^{-1/2}}{\sum_{m=0}^{N}\left[1-\left(\frac{m\pi}{ka}\right)^2\right]^{-1/2}}\right\} \tag{10}$$

and

$$TL = -10\log\left\{\frac{1}{N+1}\left[\exp(-2\Gamma_0^r L) + \sum_{m=1}^{N}\left[\frac{(r_w - ka/m\pi)^2 + x_w^2}{(r_w + ka/m\pi)^2 + x_w^2}\right]^{\frac{L}{a\sqrt{(ka/m\pi)^2-1}}}\right]\right\}. \tag{11}$$

2.1.3. *A point source*

For the comparison between experiment and prediction that will later be presented, one requires the incident sound field generated by a point volume source on one of the duct walls, since this is readily predictable and fairly easily measurable. In this case,

$$\langle\overline{p_m^2}\rangle_{in} = \overline{p_0^2}(k/k_m)^2/\Lambda_m, \quad \text{where} \quad \Lambda_m = 1,\ m = 0; = 1/2,\ m \neq 0 \tag{12}$$

and $\overline{p_0^2}$ is the mean-squared sound pressure in the fundamental mode. Again following the above arguments, one has

$$LPD = -10\log$$

$$\left\{\frac{\exp(-2\Gamma_0^r L) + \sum_{m=1}^{N}\dfrac{1}{\Lambda_m[1-(m\pi/ka)^2]}\left[\dfrac{(r_w - ka/m\pi)^2 + x_w^2}{(r_w + ka/m\pi)^2 + x_w^2}\right]^{\frac{L}{a\sqrt{(ka/m\pi)^2-1}}}}{\sum_{m=0}^{N}\dfrac{1}{\Lambda_m[1-(m\pi/ka)^2]}}\right\} \tag{13}$$

and

$$TL = -10\log$$

$$\left\{\frac{\exp(-2\Gamma_o^r L) + \sum_{m=1}^{N}\dfrac{1}{\Lambda_m[1-(m\pi/ka)^2]^{1/2}}\left[\dfrac{(r_w - ka/m\pi)^2 + x_w^2}{(r_w + ka/m\pi)^2 + x_w^2}\right]^{\frac{L}{a\sqrt{(ka/m\pi)^2-1}}}}{\sum_{m=0}^{N}\dfrac{1}{\Lambda_m[1-(m\pi/ka)^2]^{1/2}}}\right\}. \tag{14}$$

2.2. DIFFRACTION EFFECTS AT THE SILENCER TERMINATIONS

Although the effects of ray diffraction at the silencer terminations are neglected in the present formulation, a consideration of these effects will enable one to gain at least a qualitative understanding of the lower frequency limit of validity of ray models. It will perhaps be sufficient for this purpose to consider a simpler problem: the reflection of a plane wave from an infinite plane that is

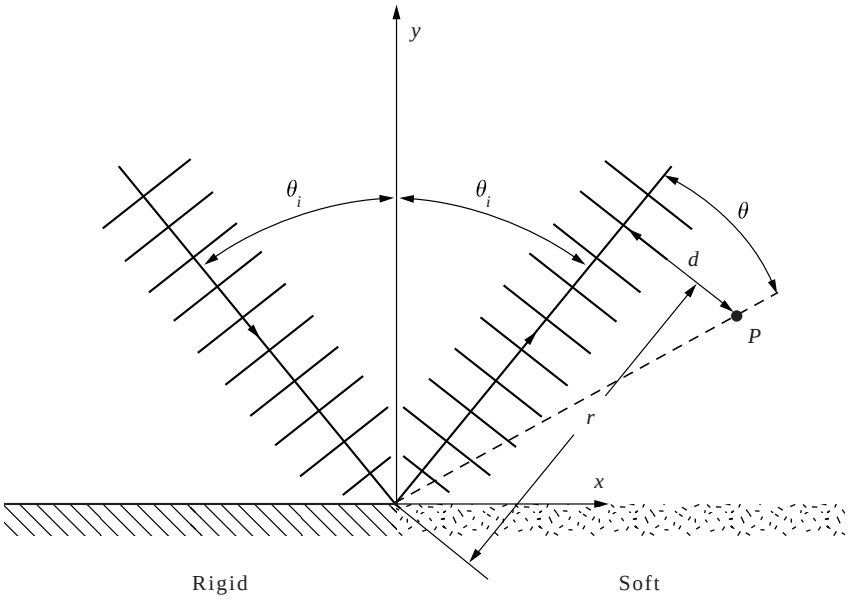

Figure 2. A plane wave incident on a half-rigid, half-soft plane.

half-rigid and half-soft, with a locally reacting surface. Various treatments of this geometry have appeared in the literature but the analysis of Morse and Ingård [16] (Chapter 8) is particularly appropriate and yields a simple result, which is adequate to illustrate the diffraction phenomenon. The geometry is shown in Figure 2. A plane wave is incident on the discontinuity between the hard and soft parts of the plane, at angle θ_i to the normal. The quantity of interest is the sound pressure amplitude of the reflected wave (also travelling at angle θ_i) at distance r from the discontinuity, along a wavefront, with d being the co-ordinate of a point P along the wavefront as shown. The result of solving the integral equation for this problem by the use of the Wiener–Hopf technique (for large kr) yields an expression for the sound pressure amplitude P_r reflected when a wave of unit amplitude is incident,

$$P_r \underset{kr\to\infty}{\longrightarrow} \left\{ \begin{array}{l} 1 - \dfrac{\beta}{2(\cos\theta_i + \beta)}\{[1 - C(u) - S(u)] + i[C(u) - S(u)]\}, \quad d < 0 \\ \dfrac{\cos\theta_i - \beta}{\cos\theta_i + \beta} + \dfrac{\beta}{2(\cos\theta_i + \beta)}\{[1 - C(u) - S(u)] + i[C(u) - S(u)]\}, \; d > 0 \end{array} \right\}, \tag{15}$$

where $u = (kd/\sqrt{2kr})^2$, β is the dimensionless admittance (referred to ρc) of the soft part of the plane and $C(u)$, $S(u)$ are Fresnel integrals (see for example the book by Abramowitz and Stegun [17]). This expression is clearly not valid for $d = 0$, where a discontinuity in reflected pressure amplitude is forecast, but it will nonetheless predict the general behaviour of the diffracted sound field. The large kr requirement in the derivation of equation (15) is not as restrictive as it might appear in the context of duct silencers, since these formulae are required here

only to give a qualitative measure of diffraction effects, ultimately indicating that these become weaker as the frequency increases. It is worth observing that, for kd large and negative, P_r tends to unity (corresponding to reflection from a rigid plane), whereas if kd is large and positive, P_r tends toward $(\cos\theta_i - \beta)/(\cos\theta_i + \beta)$, the reflected amplitude from an infinite plane of admittance β. Quantitative predictions from equation (15) will be discussed in section 5.3.

One might note, finally, that ray diffraction effects at the silencer terminations *in situ* can alternatively be expressed—with greater precision—in terms of higher order acoustic modes in both the lined and unlined duct sections. That is to say, the highly complex patterns that would arise near the terminations, particularly after successive reflections of the diffracted sound fields from the duct walls, are equivalent to sums of higher order acoustic modes (see section 3).

3. A MODE-MATCHING FORMULATION

Here, expressions for the sound fields in regions 1, 2 and 3 respectively are written as

$$p_1 = e^{i\omega t}\sum_{m=0}^{\infty}\Psi_m(y)(P_{1i}^m\, e^{-i\alpha_m x} + P_{1r}^m\, e^{i\alpha_m x}), \tag{16a}$$

$$p_2 = e^{i\omega t}\sum_{m=0}^{\infty}\Phi_m(y)(P_{2i}^m\, e^{-i\beta_m x} + P_{2r}^m\, e^{i\beta_m x}), \quad p_3 = e^{i\omega t}\sum_{m=0}^{\infty}\Psi_m(y)P_{3i}^m\, e^{-i\alpha_m x'}, \tag{16b, c}$$

where $\Psi_m(y) = \cos(m\pi y/a)$ and $\Phi_m(y) = \cos(\gamma_m y) + A_m \sin(\gamma_m y)$, γ_m being the transverse wavenumber in the silencer section and A_m a constant. Subscripts i and r denote incident and reflected waves, respectively. The duct is (as before) assumed to be anechoically terminated at both ends, so that not only are there no reflected modes in the silencer outlet section, but the reflected modes in the inlet section do not return to the silencer. One finds γ_m from solutions of the eigenequations

$$\tan(\gamma_m a/2) - iz_w\gamma_m/k = 0 \text{ (antisymmetrical modes)}, \tag{17a}$$

$$\cot(\gamma_m a/2) + iz_w\gamma_m/k = 0 \text{ (symmetrical modes)}. \tag{17b}$$

These equations were solved by the use of Muller's method. This process, together with the following mode-matching procedure, was carried out at a series of closely spaced frequencies over the range of interest. At the three lowest frequencies, the solutions of equations (17a, b) were begun for a 1-mm thickness of absorbent and the thickness increased, by 120 increments, up to the actual lining thickness. The iterated set of wavenumbers at each thickness increment was used as the set of initial values for the subsequent increment. For the smallest thickness, the rigid-wall wavenumbers were used. For frequencies higher than the lowest three values, extrapolation of the wavenumber of each mode from the previous three frequencies was achieved by the use of a quadratic polynomial, and the extrapolated value was used as a starting value in Muller's method. This was done for all modes included in the solution.

Mode-matching was achieved by carrying out a least-squares match of sound pressure and axial particle velocity at $x = 0$ and $x = L$. In the case of sound pressure, the square of the sound pressure jump for a finite sum of $M + 1$ modes at (for example) $x = 0$ was integrated across the duct width and then minimized with respect to P_{2i}^n. The jump in axial particle velocity at $x = 0$ was treated in the same way. The same process was carried out at $x = L$, but now the minimization was with respect to P_{2r}^n. Thus, for example at $x = 0$, one has for sound pressure

$$\varepsilon_1 = \sum_{m=0}^{M} (P_{2i}^m + P_{2r}^m)\Phi_m(y) - \sum_{m=0}^{M} (P_{1i}^m + P_{1r}^m)\Psi_m(y),$$
$$D_1 = \int_0^a \varepsilon_1^2 \, \mathrm{d}y, \quad \partial D_1/\partial P_{2i}^n = 0, \quad \text{i.e.,} \quad 2\int_0^a \varepsilon_1 \frac{\partial \varepsilon_1}{\partial P_{2i}^n} \mathrm{d}y = 0, \tag{18}$$

with $n = 0, 1, \ldots, M$. This should yield a "best" set of transmitted modes at $x = 0$, and gives rise to $M + 1$ equations in the $2M + 2$ unknown modal pressure coefficients P_{2i}^m and P_{1r}^m:

$$P_{2i}^n(a\Lambda_n) - \sum_{m=0}^{M} P_{1r}^m \int_0^a \Phi_n \Psi_m \, \mathrm{d}y$$
$$= \sum_{m=0}^{M} P_{1i}^m \int_0^a \Phi_n \Psi_m \, \mathrm{d}y - P_{2r}^n(a\Lambda_n), \quad n = 0, 1, \ldots, M, \tag{19}$$

where

$$\Lambda_n = \frac{1}{a}\int_o^a \Phi_n^2 \, \mathrm{d}y. \tag{20}$$

For axial particle velocity, one has, as above,

$$\varepsilon_2 = \frac{1}{\omega\rho}\left[\sum_{m=0}^{M} \beta_m (P_{2i}^m - P_{2r}^m)\Phi_m(y) - \sum_{m=0}^{M} \alpha_m (P_{1i}^m - P_{1r}^m)\Psi_m(y)\right],$$
$$D_2 = \int_0^a \varepsilon_2^2 \, \mathrm{d}y, \quad \partial D_2/\partial P_{2i}^n = 0, \quad \text{i.e.,} \quad 2\int_0^a \varepsilon_2 \frac{\partial \varepsilon_2}{\partial P_{2i}^n} \, \mathrm{d}y = 0, \tag{21}$$

and so

$$P_{2i}^n(a\beta_n\Lambda_n) + \sum_{m=0}^{M} P_{1r}^m \alpha_m \int_0^a \Phi_n \Psi_m \, \mathrm{d}y$$
$$= \sum_{m=0}^{M} P_{1i}^m \alpha_m \int_0^a \Phi_n \Psi_m \, \mathrm{d}y + P_{2r}^n(a\beta_n\Lambda_n), \quad n = 0, 1, \ldots, M. \tag{22}$$

Equations (19) and (22) constitute a set of $2M + 2$ linear equations in the $2M + 2$ unknown reflected and transmitted modal coefficients at $x = 0$, upon assuming all incident modal coefficients in region 1 and reflected modal coefficients in region 2 are specified. The incident coefficients were readily found

here for a point source located on one of the duct walls a distance x_s from the inlet to the silencer:

$$P_{1i}^n/(\rho\omega Q_0/2Sk) = k\,\mathrm{e}^{-\mathrm{i}\alpha_n x_s}/\alpha_n \Lambda_n, \tag{23a}$$

S being the cross-sectional area of the duct and Q_0 the volume velocity amplitude of the source. In the case of the mode-matching model with equal incident modal energy density, the P_{1i}^n values were found from

$$P_{1i}^n = (P_{ref}^n/\sqrt{\Lambda_n})\,\mathrm{e}^{-\mathrm{i}\alpha_n x_s}, \tag{23b}$$

P_{ref}^n being a reference sound pressure amplitude in the nth incident mode, put equal to unity. Only propagating incident modes were included. The phase of each incident mode is dictated by the value of $\alpha_n x_s$. The equations in the unknown modal coefficients in the outlet plane, at $x = L$, are

$$-P_{2r}^n(a\,\mathrm{e}^{\mathrm{i}\beta_n L}\Lambda_n) + \sum_{m=0}^{M} P_{3i}^m \int_0^a \Phi_n \Psi_m \,\mathrm{d}y = P_{2i}^n(a\,\mathrm{e}^{-\mathrm{i}\beta_n L}\Lambda_n), \quad n = 0, 1, \ldots, M, \tag{24a}$$

$$P_{2r}^n(a\beta_n\,\mathrm{e}^{\mathrm{i}\beta_n L}\Lambda_n) + \sum_{m=0}^{M} P_{i3}^m \alpha_m \int_0^a \Phi_n \Psi_m \,\mathrm{d}y = P_{2i}^n(a\beta_n \mathrm{e}^{-\mathrm{i}\beta_n L}\Lambda_n), \quad n = 0, 1, \ldots, M, \tag{24b}$$

from continuity of sound pressure and axial particle velocity, respectively.

Initially, all P_{2r}^m values were equated to zero, and equations (19) and (22) were solved. The P_{2i}^m values were used for the set of incident modes at $x = L$, and equations (24a, b) for the reflected and transmitted modal coefficients at $x = L$ (again $2M + 2$) were solved. The P_{2r}^m values were then used in the equations at the inlet to find new. P_{2i}^m values, and the process was repeated until the modal coefficients ceased to change significantly. This iterative process reduced the number of equations to be solved simultaneously by a factor of two and, since only a small number of iterations was required, considerably reduced the computation time. A sufficiently large value of M was taken, so that the solution had converged adequately. A further reduction in computing time was achieved here by separately matching the odd and even modal components in the sound field so that, instead of solving a set of $2M + 2$ equations, two sets of $M + 1$ equations were solved at each iteration. The value of M was put equal to the number of propagating modes at the particular frequency, plus a further number of modes. This additional number was put equal to 9 in the computed data presented here, and proved sufficient to ensure reasonable convergence of the solution.

Once the modal coefficients had been determined, it was a straightforward matter to compute both the LPD and TL of the silencer. These quantities were found from the coefficients of the propagating modes incident on, and transmitted by, the silencer. In the mode-matching model, modes are reflected

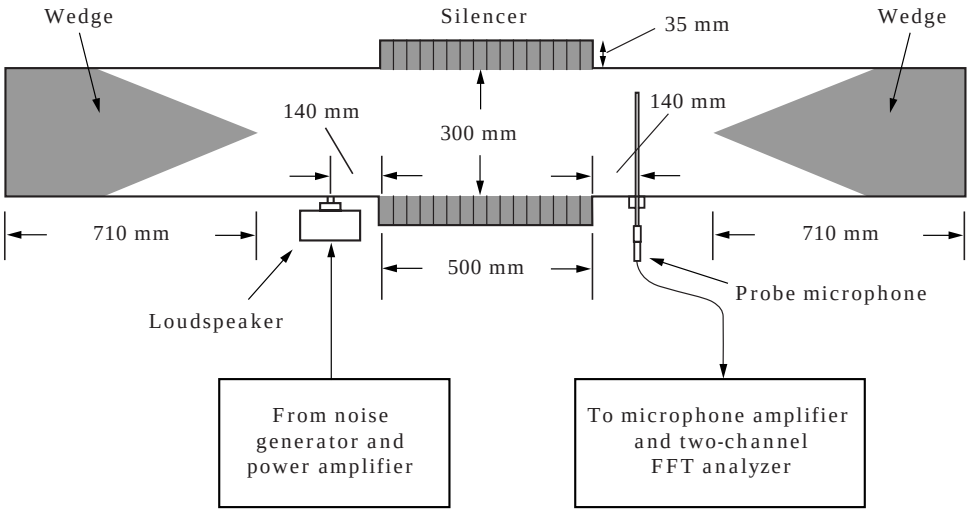

Figure 3. Experimental duct apparatus.

from the silencer inlet and outlet, in contrast to the ray model, though as far as the *LPD* and *TL* are concerned, their role is only in determining the transmitted modal coefficients.

4. EXPERIMENTS

To verify the predictions of the ray model by comparison to experimental data, a two-dimensional duct test apparatus was fabricated. A plan view of this is shown in Figure 3. The height of the duct was 25 mm, enabling two-dimensional mode propagation to occur up to about 6·9 kHz. The source loudspeaker—a medium-sized pressure driver—was connected to the duct by a 10-mm diameter hole located halfway along the 25-mm duct wall (this arrangement being intended to simulate the aforementioned point source), and so only even modes in this dimension should, in theory, have been excited. Consequently the frequency range for two-dimensional modes was from 0 to 13·8 kHz. Non-idealities in construction of the duct would, in reality, impose a rather lower limit and experimental data were taken only up to 7·5 kHz. The soft walls in the silencer section consisted of a 35-mm thickness of partially reticulated polyurethane foam with a steady flow resistivity of 4390 mks rayl/m. The bulk acoustic properties of the foam—required to determine the normal surface impedance of the liner—were found by means of an impedance tube, from tests on two differing thicknesses of absorbent. The foam was cut into sections 25 mm wide, and these were separated by thin aluminium baffles placed transverse to the duct axis, to prevent wave propagation along the liner and render it essentially point reacting. These baffles would cease to be completely effective for this purpose much above about 7 kHz, although no really sudden

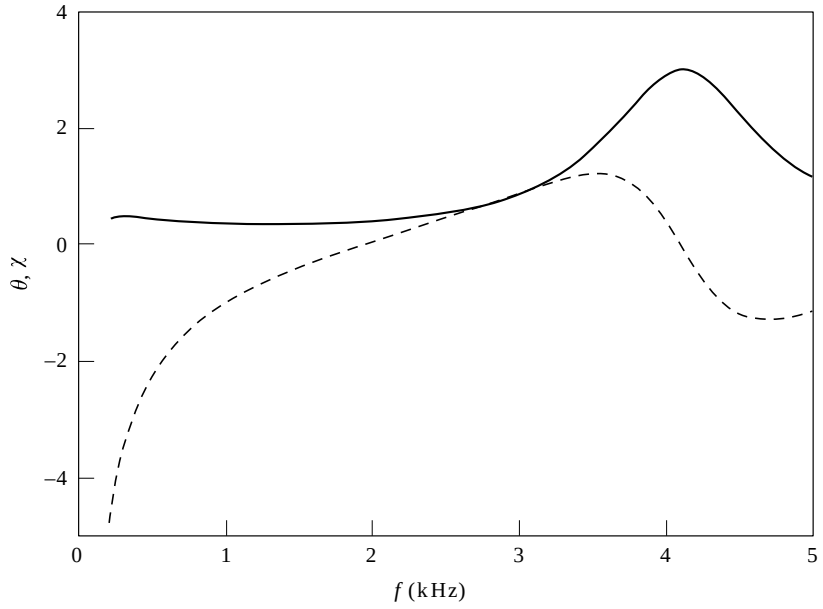

Figure 4. Predicted normal impedance z_w of the experimental duct lining against a rigid backing, in ρc units: ————, resistance r_w;- - - - - reactance x_w.

departure from point reacting behaviour would be anticipated at rather higher frequencies. The normal impedance (in ρc units) of the acoustic lining with its rigid backing, predicted from the bulk acoustic properties of the foam, is plotted in Figure 4 from 200 Hz to 5 kHz. We note that, from about 1 to 3 kHz, $|z_w| < 1$, i.e., the walls are fairly "soft" over this frequency range.

Random noise was fed from an amplifier to the speaker and the sound field was sampled by means of a probe microphone at 20-mm intervals. Single frequency sound pressure level data (in the form of a transfer function, referred to the voltage input to the speaker) were obtained from an FFT analyzer and spatially averaged mean-squared pressure figures were found at each frequency. The silencer section could be removed, thereby permitting measurement of the sound pressure level with no silencer present. The *IL* of the silencer could thus be found directly by means of this duct apparatus.

5. NUMERICAL AND EXPERIMENTAL RESULTS

In this section, the mode-matching formulation is first verified by comparison to experimental data of the *LPD* with a point source, and comparison is made to *LPD* predictions from the ray model. Then a series of comparisons is made between mode and ray predictions of *TL* and *LPD* for an incident sound field with equal acoustic energy density distribution in the modes. Finally, some diffraction patterns are presented for a range of frequencies and these are viewed in the light of the previous comparisons between ray and mode predictions, with

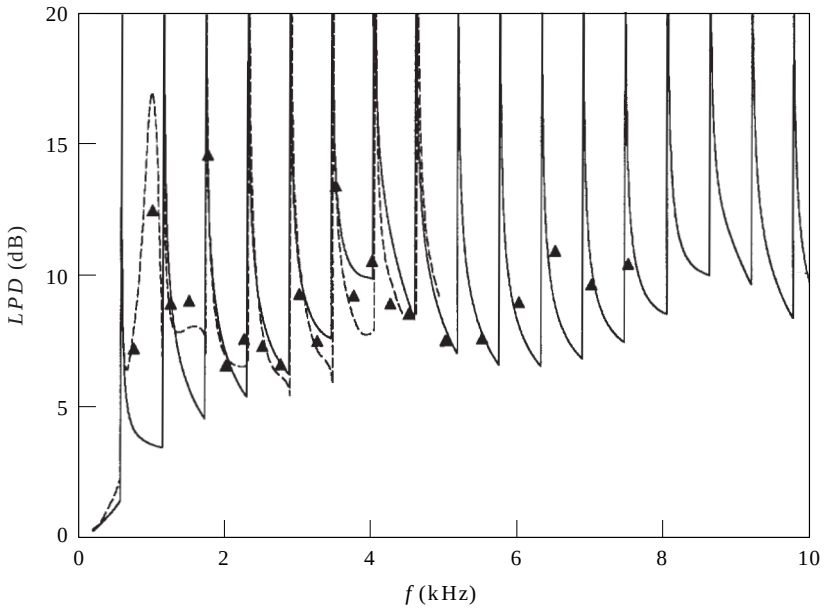

Figure 5. Predicted and experimental *LPD* for the test duct with a point source: ————, ray model; - - - - -, mode-matching model, ▲ measured data.

the object of establishing their relevance to a lower frequency limit on the range of validity of ray models.

5.1. COMPARISON BETWEEN *LPD* PREDICTIONS AND MEASUREMENTS

The normal surface impedance of the experimental silencer was predicted *via* the bulk acoustic properties of the foam, from $z_w = z_a \coth \Gamma\ell$, z_a and Γ being the dimensionless characteristic impedance and the dimensional propagation coefficient respectively, and ℓ the liner thickness. Predictions were made of the *LPD* of the silencer from 200 Hz to 10 kHz by the ray theory, and from 200 Hz to 4·9 kHz by the mode-matching theory. This upper frequency limit was imposed by the maximum allowable size of argument of exponential functions used in the computer routines for circular functions with complex argument, employed in the eigenequations (17a, b). A large imaginary part in the transverse wavenumber of a mode in the lined duct section could cause overflow in execution of the program. This could, perhaps, have been overcome by a re-formulation of the problem, but the effort involved in this was not considered worthwhile, since multimode predictions up to about 5 kHz were deemed to be adequate for the purpose in the present investigation.

Comparison is made between the two *LPD* predictions and measured data in Figure 5. It can be seen that the *LPD* predicted by both methods exhibits a series of (theoretically infinite) peaks at the cut-on frequencies of higher modes in the inlet and outlet ducts. The minimum *LPD* values, between these peaks, are all less than about 10 dB. The mode-matching predictions are in excellent

agreement with the measured data up to 4·5 kHz (at which frequency 9 modes propagate). Below about 1·8 kHz, the ray theory does not predict the minimum *LPD* values accurately, but this would not be expected in view of the various approximations upon which it relies. Above this frequency, it is in good agreement with the mode-matching theory. Above 5 kHz, the ray theory is in excellent agreement with the measured data. We note undulations in the

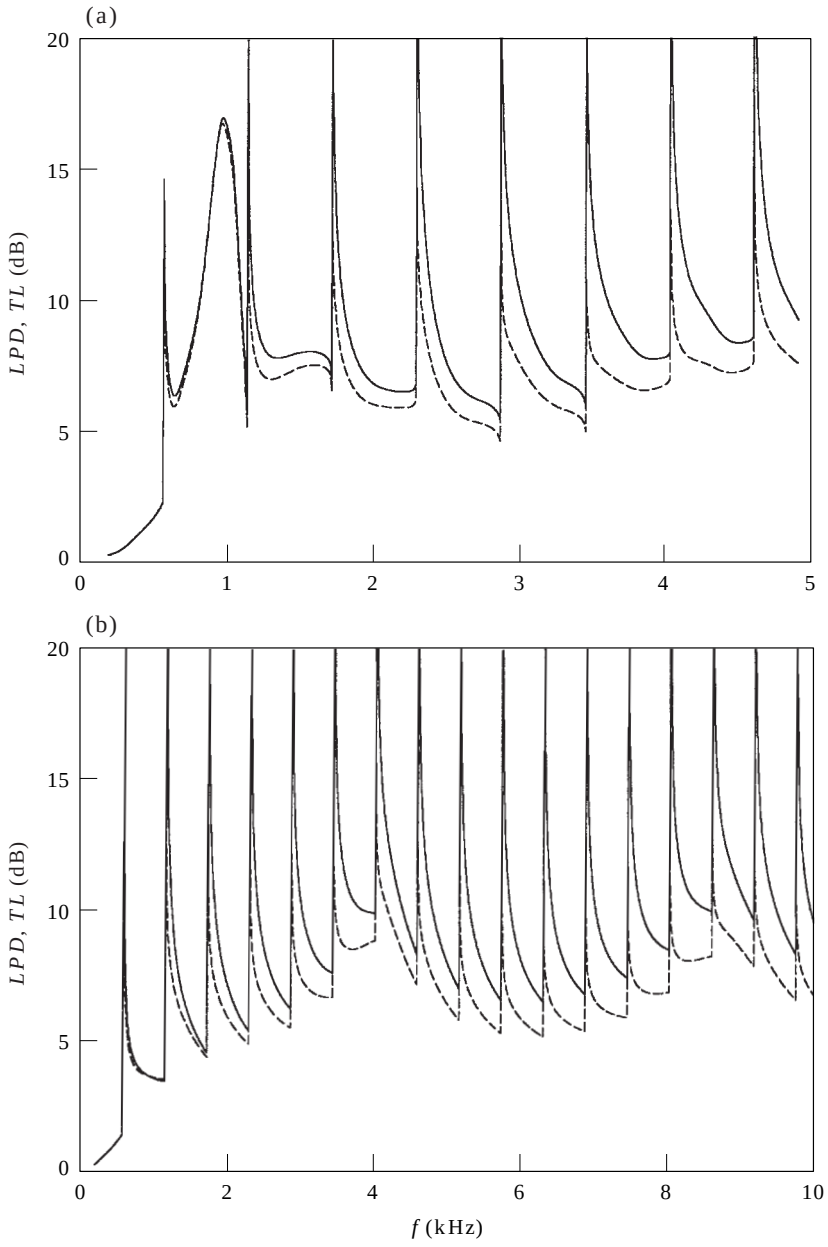

Figure 6. Predicted *LPD* and *TL* for the test duct with a point source. (a) mode-matching model, (b) ray model; ————, *LPD*; - - - - -, *TL*.

envelope of the minimum values of the *LPD*, more obviously in the ray theory predictions. These can be qualitatively explained by plotting the curve of the energy absorption coefficient of a wall in region 2 for $\theta = 45°$ (chosen as a representative angle of incidence) *versus* frequency. This curve (not shown here for the sake of clarity) tends to follow the same pattern. One can see from equation (13) that a high wall absorption coefficient implies a high *LPD* figure, at least on the basis of the ray model. The numerical predictions from the mode-matching model appear to follow this trend too, in the range 2–5 kHz.

5.2. SOME NUMERICAL PREDICTIONS FOR THE TEST DUCT

In this section, predicted *LPD* and *TL* data are presented for the test silencer—both as it was in the experiments and with various changes, e.g., different values of x_s and L—and for a more practical type of silencer. Two different assumptions are made about the incident sound field: modes from a point source and equal energy density in all incident modes.

5.2.1. *The point source*

Comparisons are made between the predicted *LPD* and *TL* for the test duct in Figure 6(a, b), from both the mode-matching model and the ray model. The values of x_s and L are as they were in the experiments. The results from the mode-matching model are shown in Figure 6(a), the frequency range being 0–5 kHz. The general shapes of the plots are very similar, although the *TL* figures are lower than the *LPD* values. The ray model results are plotted over the range 0–10 kHz in Figure 6(b). Again, the *TL* curve is lower than the *LPD* curve, and the two plots are of similar shape. Both *TL* and *LPD* curves in Figures 6(a, b) exhibit sharp (theoretically infinite) peaks at modal cut-on frequencies.

5.2.2. *Equal energy density in the incident modes*

Neise *et al.* [18], in a theoretical and experimental study of fan noise propagation in rectangular ducts, have shown that equality of energy density amongst propagating modes best represents a multimode sound field. As mentioned in section 2.1.1, this also implies equality of space-averaged mean-squared sound pressure over the propagating modes, and equations (7) and (8) may be employed to give ray model predictions for the *LPD* and *TL* respectively. Since fan noise is usually the dominant noise source in air-moving ducts (perhaps the main application of the present work), it is appropriate to assume equality of modal energy density as a typical representation of a realistic sound field.

Ray model predictions of *LPD* and *TL* for the test duct with equal energy density in all incident modes are shown in Figure 7. Again, the *TL* curve lies below the *LPD* curve, but this time neither the *TL* nor the *LPD* curves show the peaks at modal cut-on that are characteristic of the point source plots of Figures 5 and 6(a, b). Instead, the *LPD* shows a small step increase with rising frequency and the *TL* merely a slight kink.

In the case of the mode-matching model, the predicted *LPD* and *TL* depend on the relative phases of the incident modes (whereas the ray model does not

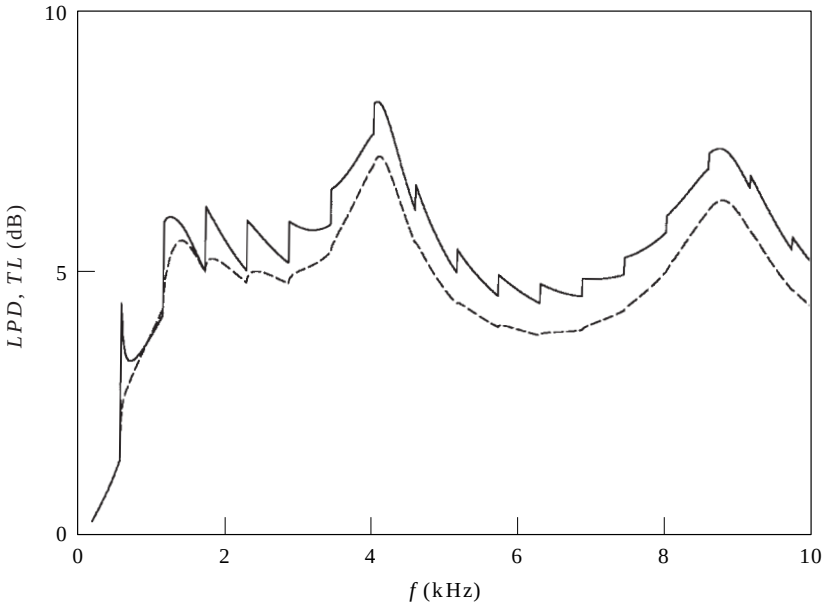

Figure 7. Predicted *LPD* and *TL* for the test duct with equal energy density in all incident modes: ————, *LPD*;- - - - -, *TL*.

distinguish between them). This is easily seen if the incident and transmitted sound fields are related *via* a (square) transmission matrix $[\mathbf{T}] \equiv [T_{ij}]$ of size $M + 1$,

$$\{P^i_{3i}\} = \begin{Bmatrix} P^0_{3i} \\ \cdot \\ \cdot \\ \cdot \\ P^M_{3i} \end{Bmatrix} = [T_{ij}] \begin{Bmatrix} P^0_{1i} \\ \cdot \\ \cdot \\ \cdot \\ P^M_{1i} \end{Bmatrix} = [T_{ij}]\{P^i_{1i}\}, \tag{25}$$

where $\{P^i_{3i}\}$ and $\{P^i_{1i}\}$ are column vectors containing the transmitted and incident modal coefficients respectively. The elements of [**T**] are not of course dependent on the incident or transmitted sound fields, but only on the silencer parameters. Clearly, each transmitted modal coefficient will be dependent not only upon the moduli of *all* the incident (complex) modal coefficients, but also on their phases. This modal coupling occurs at the silencer terminations. In the ray model, the relative phases of the incident modes are immaterial, since acoustic reflection at the silencer terminations is ignored.

Mode-matching predictions—with equal energy density in all incident modes—of the *TL* for the test silencer with $L = 0{\cdot}5$ m are plotted in Figure 8(a), for five different values of x_s: 0, 0·14, 0·3, 0·6, and 1·0 m. These values—apart from the first and second—were arbitrarily selected. For $x_s = 0$, all incident modes are in phase (see equation (23b)), though for the other values of x_s, the relative modal phase is governed by α_n for each mode. The most obvious feature of the curves in Figure 8(a) is that the *TL* for $x_s = 0$ is significantly higher,

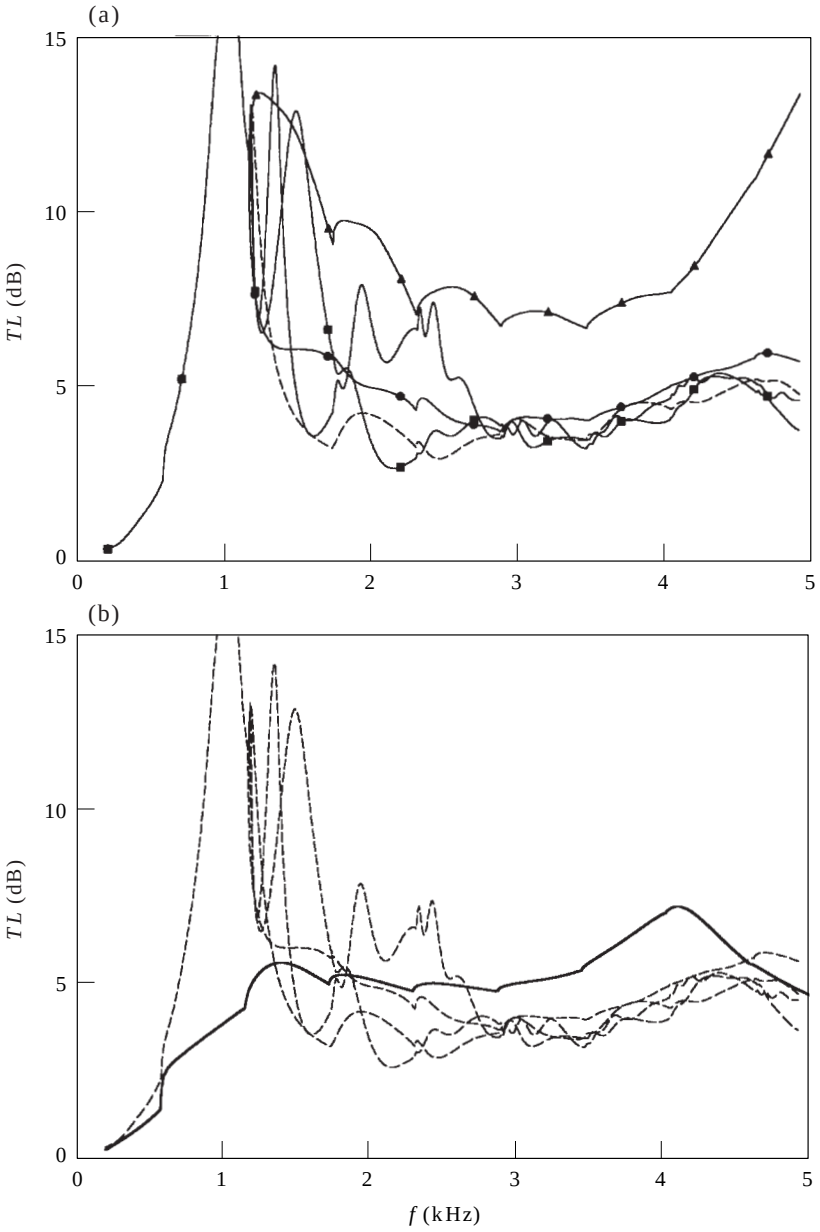

Fig. 8(a–b).

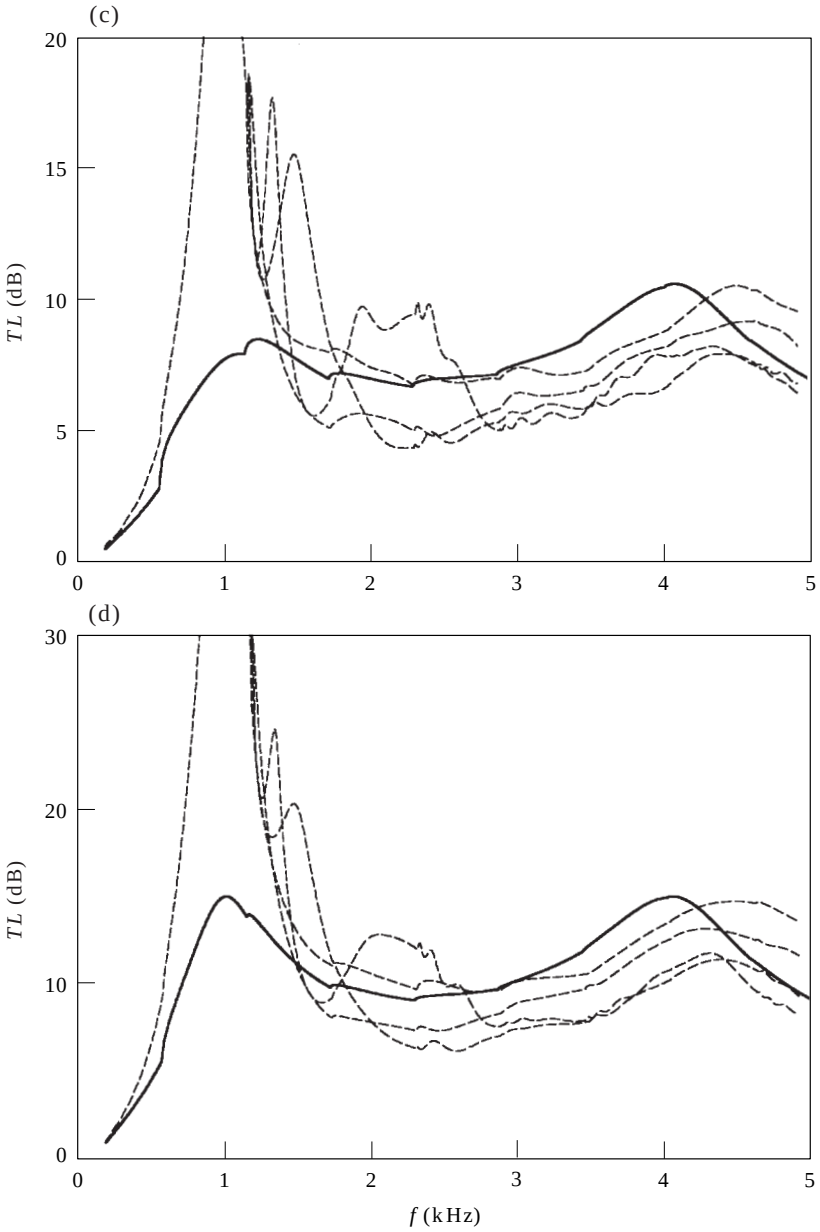

Fig. 8(c–d).

Figure 8. Mode-matching and ray predictions of *TL* for the test duct (equal energy density in all incident modes), with varying duct lengths and source positions: (a) mode-matching predictions for $L = 0{\cdot}5$ m: —▲—, $x_s = 0$, —●—, $x_s = 0{\cdot}14$ m,- - - - -, $x_s = 0{\cdot}3$ m,—■—, $x_s = 0{\cdot}6$ m, ————, $x_s = 1{\cdot}0$ m; (b) $L = 0{\cdot}5$ m, (c) $L = 1{\cdot}0$ m, (d) $L = 2{\cdot}0$ m:- - - - -, mode-matching predictions for various values of x_s from 0·14 to 1·0 m; ————, ray predictions.

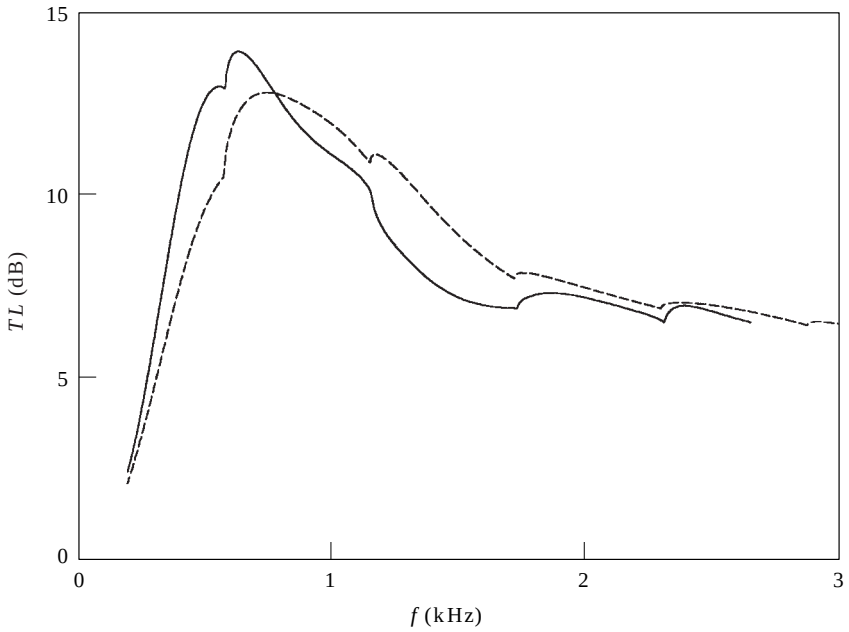

Figure 9. Mode-matching and ray predictions (with equal energy density in all incident modes) of TL for a duct with $a = 0{\cdot}3$ m, $L = 0{\cdot}5$ m, $x_s = 0{\cdot}14$ m and a 0·1-m thick lining of fibrous material against a rigid backing; flow resistivity of lining material = 10^4 mks rayl/m: ————, mode-matching model; - - - - -, ray model.

above 1·5 kHz, than the other curves, which lie fairly close together. The reason for this is not clear, but it is obviously very unlikely in practice for the phases of the incident modes all to be the same. Therefore, the plot for $x_s = 0$ is regarded as being unrealistic, and the TL range spanned by the other curves is taken to be more representative of a typical incident sound field. In Figure 8(b), the curves for $x_s \neq 0$ (not shown here by different symbols) are compared to the ray theory and reasonable agreement—to within 2–3 dB—is noted above about 1·8 kHz.

Comparisons of mode-matching TL predictions for $x_s = 0{\cdot}14$ m, ..., 1·0 m (as in Figure 8(b)) and ray predictions are shown in Figure 8(c) for $L = 1{\cdot}0$ m and in Figure 8(d) for $L = 2{\cdot}0$ m. Good agreement between ray and mode-matching predictions is noted. A comparison between mode-matching and ray predictions (as before, with equal energy density in all incident modes) is shown in Figure 9, for a duct with a liner that is more representative of practical types of absorbent. Here, $a = 0{\cdot}3$ m, $L = 0{\cdot}5$ m, $x_s = 0{\cdot}14$ m (in the case of the mode-matching predictions), the liner is fibrous and its thickness and steady flow resistivity are 0·1 m and 10^4 mks rayl/m respectively. The bulk properties of this lining material were found by the use of the empirical formulae of Delany and Bazley [19]. Agreement between the two methods is very close in this case, certainly within 1–2 dB over most of the frequency range. Even at low frequencies, the ray predictions are in good agreement with the mode-matching theory. A

possible reason for this better agreement—as compared to that for the experimental duct—is given in section 5.3.

5.3. DIFFRACTION EFFECTS

In section 2.2, some consideration was given to diffraction effects at the junction between the rigid and soft parts of the duct. While this can only give an indication of wave scattering effects at the silencer inlet and outlet, it is worth discussing some representative diffraction patterns with the main objective of establishing that diffraction effects are small at sufficiently high frequencies. Expressions (15) are particularly relevant to the inlet, but cannot be used to represent the sound pressure pattern in a ray after the second reflection from the duct walls, since specular reflection will only occur for a plane incident wave—an incident diffracted wave field would become distorted upon reflection from a soft wall. Even so, an indication of the diffraction effects in the incident wave before the second reflection for a range of frequencies is of interest. Plots of $|P_r|$ (for unit incident pressure amplitude) versus θ are shown in Figures 10(a–d), for $r = 1$ m, $\theta_i = 45°$ (a representative angle), a soft wall with the same impedance as that in the experimental duct and at a range of frequencies. This value of r is chosen simply so that $kr > 20$ (a suitably large value) for all frequencies of interest. It should be noted that, as r increases, the diffraction peaks and troughs all move toward θ, $= 0°$, i.e., the diffraction pattern "shrinks" laterally. This can be appreciated from the definition of u. The discontinuity in $|P_r|$ at $\theta = 0°$ can be clearly seen. The dashed lines in Figures 10(a–d) show the limiting value of $|P_r|$ as $kd \to \pm\infty$, and correspond to plane-wave reflection from a rigid or soft surface, as discussed in section 2.2; they represent to the "ideal" high-frequency case in ray acoustics, where diffraction effects are absent. For $f = 1{\cdot}25$ kHz, diffraction effects can be seen to dominate the pressure pattern within the range $\theta \approx \pm 25°$, with large deviations from the ideal asymptotic step change in $|P_r|$, and it is not surprising that the ray acoustics approximation begins to break down at the lower frequencies. At 2·5 kHz, however, the diffraction-dominated region is only within the region $\theta \approx \pm 18°$. A better approach to ray behaviour might be expected, consistent with the better agreement between ray and mode models for the TL at this higher frequency. At 5 kHz, the pressure pattern can be seen to be considerably closer to the ideal, and at 10 kHz, even more so. The pattern of $|P_r|$ is not very sensitive to θ_i; plots for $\theta_i = 0°$ were very similar to those in Figures 10(a–d), and so are not shown. Further diffraction patterns are shown in Figures 11(a–d). This case is that of Figures 10(a–d), but with a wall impedance corresponding to the plots in Figure 9, with a 0·1-m thick fibrous absorbent placed against a rigid backing. This absorbent is closer to a practical case than the plastic foam used in the experimental duct. One can note that, at 1·25 kHz, diffraction effects are significantly less pronounced than with the plastic foam absorbent, and the same is true—but to a lesser extent—at 2·5 kHz. The patterns at 5 and 10 kHz are similar for the two liners.

The data shown here are broadly in keeping with the quality of agreement between the ray and mode TL predictions at different frequencies. For example, the weaker diffraction effects at 1·25 kHz in the case of the fibrous lining are

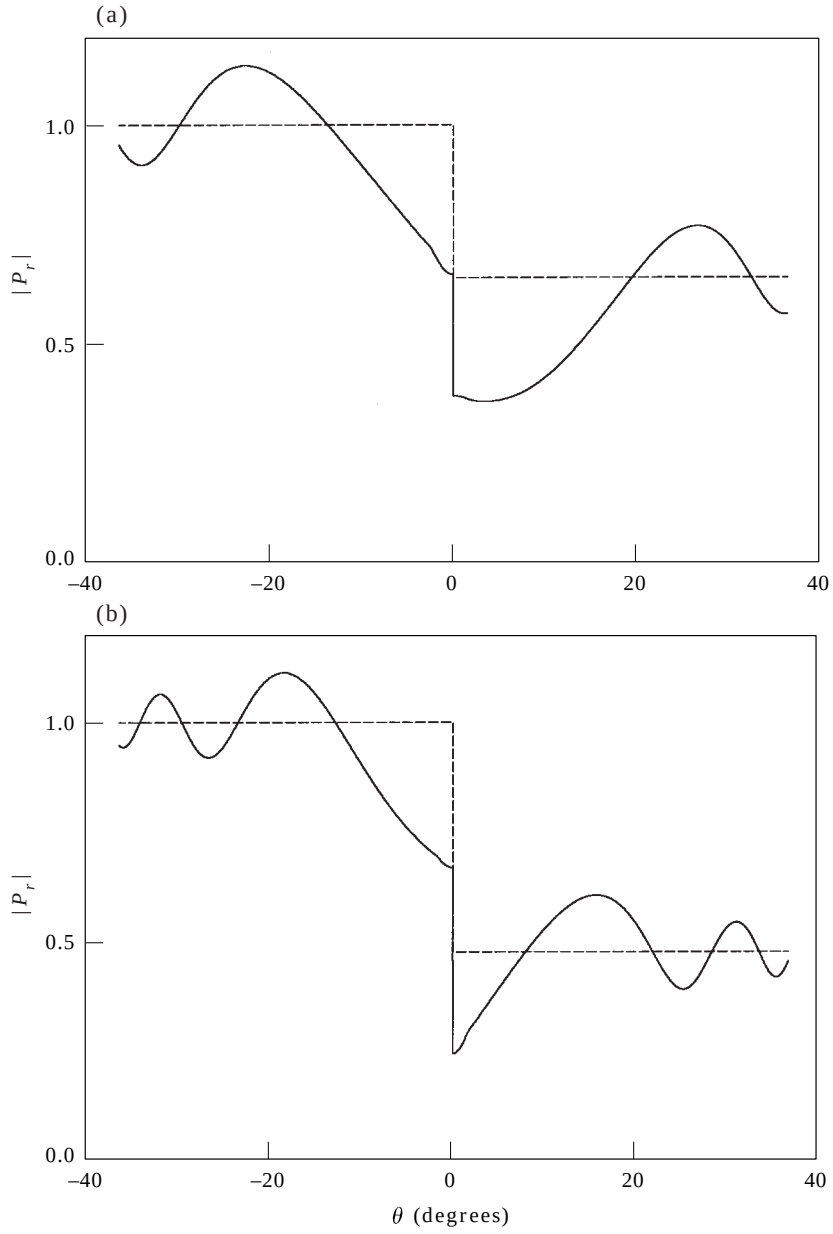

Fig. 10(a–b).

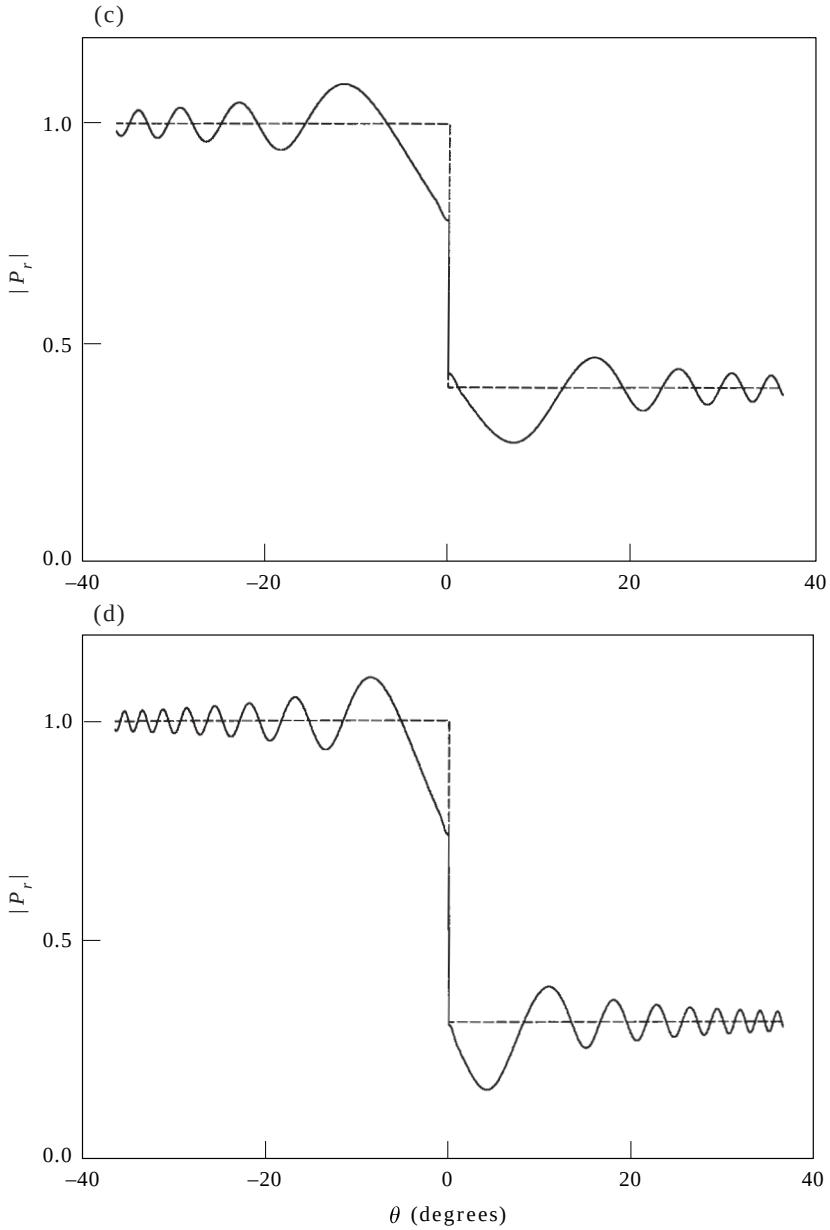

Fig. 10(c–d).

Figure 10. Diffraction pattern for a plane wave of unit sound pressure amplitude, incident upon a half-rigid, half-soft plane (see Figure 2 for geometry), $r = 1$ m, $\theta_i = 45°$; impedance of soft half is that of the experimental duct lining: ————, predicted $|P_r|$ (expressions (15)); - - - - -, $|P_r|$ for reflection from infinite rigid and infinite soft surfaces. (a) $f = 1{\cdot}25$ kHz; (b) $f = 2{\cdot}5$ kHz; (c) $f = 5$ kHz; (d) $f = 10$ kHz.

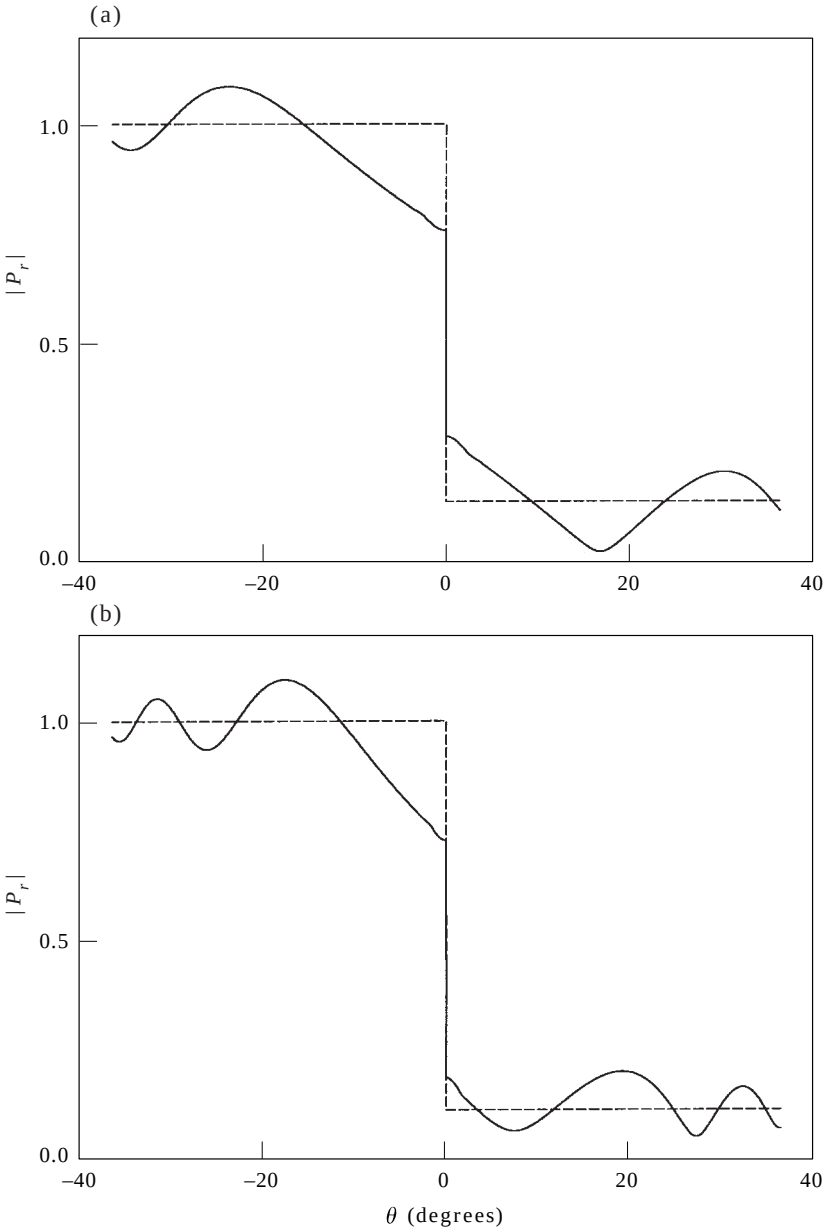

Fig. 11(a–b).

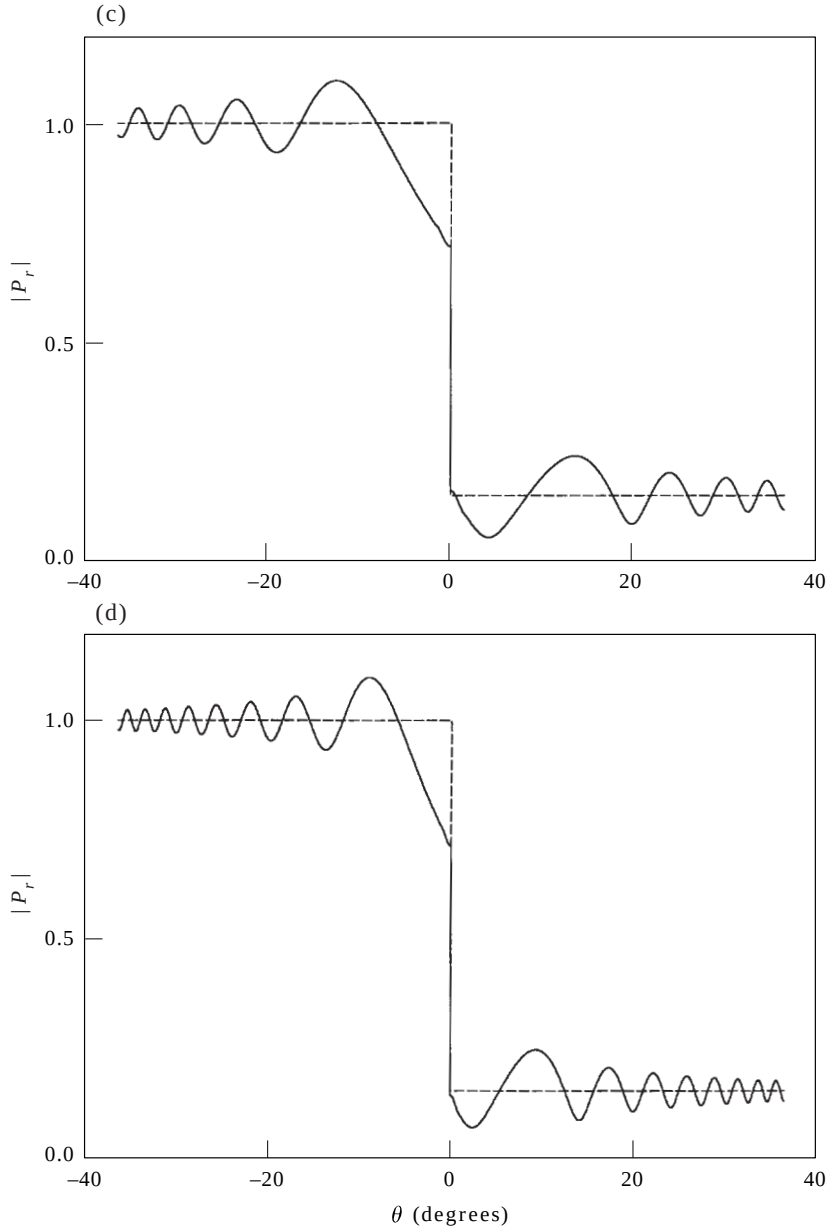

Fig. 11(c–d).

Figure 11. Diffraction pattern for a plane wave of unit sound pressure amplitude, incident upon a half-rigid, half-soft plane (see Figure 2 for geometry), $r = 1$ m, $\theta_i = 45°$; impedance of soft half is that of the duct lining in Figure 9: ————, predicted $|P_r|$ (expressions (15)); - - - - -, $|P_r|$ for reflection from infinite rigid and infinite soft surfaces. (a) $f = 1{\cdot}25$ kHz; (b) $f = 2{\cdot}5$ kHz; (c) $f = 5$ kHz; (d) $f = 10$ kHz.

consistent with the very significantly better agreement between ray and mode predictions—evident in Figure 9—than that in Figures 8(b–d). It is difficult to give any very general guidelines about the lower frequency limit of applicability of ray models, because this will depend on the wall impedance and how it changes with frequency. However, the plots shown here qualitatively support the physical arguments that diffraction effects should become unimportant at high frequencies, where ray acoustics is a valid approximation.

6. DISCUSSION AND CONCLUSIONS

The very simple multimode ray model that has been described has given gratifyingly accurate predictions of the *LPD* as compared to the more complete mode-matching model and to measured data, in a particularly difficult comparison involving a point sound source. It was not considered necessary to make comparisons between the two models and experimental data with equipartition of energy density between the incident modes—a more realistic assumption in practical situations—and in any case, it would have been difficult to generate this kind of sound field in the experimental system employed in this investigation.

The loss of predictive accuracy in the ray model (as compared to a more accurate formulation) would seem to be more than offset by the great ease with which it may be employed. The model involves a much more "physical"—though less precise—description of the sound field in a silencer than that embodied in the modal formulation (or, for that matter, in a fully numerical treatment such as a finite element analysis). The ray formulation—as given here—is intended to be applicable at frequencies where there are multiple propagating modes incident on the silencer. At lower frequencies, where the fundamental mode dominates the sound field in the lined duct section, the ray model would not necessarily be very accurate because of the approximate nature of the model adopted here for the fundamental mode attenuation (see equation (5)). It is not intended as a substitute for more exact treatments where accurate results are required, but neither does it fall within the category of "simplistic formulae" (all too numerous in the field of sound-absorbing ducts), which usually do not embody all the important physical features of the problem and frequently give results that are several hundred percent in error in the decibel attenuation figure. The object of the present investigation was to determine whether a ray treatment is likely to be of value as a design tool for rectangular section dissipative duct silencers (such as those in ventilation systems) at frequencies above the point where the fundamental mode is predominant. The combination of a fundamental-mode formulation—to cover the low frequency range—and a high-frequency ray model is potentially extremely useful in silencer design.

The two-dimensional ray treatment has been extended to three dimensions (though the details are not given here), and the resulting formulae are still very straightforward. The three-dimensional model has not yet been experimentally verified. Mean gas flow effects can, in principle, readily be included in the ray

model, and in order to apply ray models to practical devices such as splitter silencers, geometrical effects such as area blockage also need to be included. More complicated devices such as offset banks of splitters might also be amenable to ray treatments. Particularly if the sound fields in the inlet duct can be represented as a modal sum, the considerable flexibility of ray models may well permit the formulation of hybrid treatments such as that described here.

REFERENCES

1. A. CUMMINGS and N. SORMAZ 1993 *Journal of Sound and Vibration* **168**, 209–227. Acoustic attenuation in dissipative splitter silencers containing mean fluid flow.
2. F. P. MECHEL 1990 *Acustica* **70**, 93–111. Theory of baffle-type silencers.
3. F. P. MECHEL 1990 *Acustica* **72**, 7–20. Numerical results to the theory of baffle-type silencers.
4. N. SORMAZ, A. CUMMINGS and B. NILSSON 1992 *Proceedings of the Euronoise '92 Meeting*, *Imperial College London*, *September*. Sound attenuation in finite-length splitter silencers.
5. N. SORMAZ 1994 *Ph.D. Thesis*, *University of Hull*. Acoustic attenuation of dissipative splitter silencers.
6. R. J. ASTLEY and W. EVERSMAN 1978 *Journal of Sound and Vibration* **57**, 367–388. A finite element method for transmission in non-uniform ducts without flow: comparison with the method of weighted residuals.
7. W. EVERSMAN and R. J. ASTLEY 1981 *Journal of Sound and Vibration* **74**, 89–101. Acoustic transmission in non-uniform ducts with mean flow, part I: the method of weighted residuals.
8. R. J. ASTLEY and W. EVERSMAN 1981 *Journal of Sound and Vibration* **74**, 103–121. Acoustic transmission in non-uniform ducts with mean flow, part II: the finite element method.
9. R. KIRBY 1996 *Ph.D Thesis*, *University of Hull*. The acoustic modelling of dissipative elements in automotive exhausts.
10. B. J. TESTER 1973 *Journal of Sound and Vibration* **27**, 515–531. Ray models for sound propagation and attenuation in ducts, in the absence of mean flow.
11. B. J. TESTER 1973 *Journal of Sound and Vibration* **28**, 151–203. The propagation and attenuation of sound in lined ducts containing uniform or "plug" flow.
12. A. J. KEMPTON 1980 *Paper no. AIAA*-80-0968, *presented at the American Institute of Aeronautics and Astronautics 6th Aeroacoustics Conference*, *Hartford*, *CT*, 4–6 June. Ray theory to predict the propagation of broadband fan-noise.
13. A. J. KEMPTON 1983 *Paper no. AIAA*-83-0711, *presented at the American Institute of Aeronautics and Astronautics 8th Aeroacoustics Conference*, *Atlanta*, *GA*, 11–13 April. Ray-theory and mode-theory prediction of intake-liner performance: a comparison with engine measurements.
14. W. K. BOYD, A. J. KEMPTON and C. L. MORFEY 1984 *Paper no. AIAA*-84-2332, *presented at the American Institute of Aeronautics and Astronautics 9th Aeroacoustics Conference*, *Williamsburg*, *VA*, 15–17 October. Ray-theory predictions of the noise radiated from aeroengine ducts.
15. R. P. DOUGHERTY 1996 *Paper no. AIAA*-96-1773, *presented at the Second American Institute of Aeronautics and Astronautics/Confederation of European Aerospace Societies Aeroacoustics Conference*, *State College*, *PA*, 6–8 *May*. Nacelle acoustic design by ray tracing in three dimensions.
16. P. M. MORSE and K. U. INGÅRD 1968 *Theoretical Acoustics*. New York: McGraw-Hill.
17. M. ABRAMOWITZ and I. A. STEGUN 1965 *Handbook of Mathematical Functions*. New York: Dover.

18. W. NEISE, W. FROMMHOLD, F. P. MECHEL and F. HOLSTE 1993 *Journal of Sound and Vibration* **174**, 201–237. Sound power determination in rectangular flow ducts.
19. M. E. DELANY and E. N. BAZLEY 1970 *Applied Acoustics* **3**, 105–116. Acoustical properties of fibrous absorbent materials.